Electronic Research Archive

https://www.aimspress.com/journal/era

ERA, 34(7): 4913–4930.
DOI: 10.3934/era.2026217
Received: 22 March 2026
Revised: 11 May 2026
Accepted: 01 June 2026
Published: 08 June 2026

Research article

Adaptive maneuvering control of a quadrotor UAV using double dynamic filters

Cun Yang*

School of Mathematics and Informational Science, Shandong Technology and Business University, Yantai 264005, China

* **Correspondence:** Email: yangcongcong163@163.com.

Abstract: This paper proposes an adaptive maneuvering control for a quadrotor unmanned aerial vehicle with position constrained by geometric equations and unknown parameters. Based on the structural characteristics of the quadrotors, the inner–outer-loop controller is designed for two cascaded subsystems to solve the maneuvering problem of the position subsystem and the Euler angle tracking problem of the attitude subsystem. Meanwhile, double dynamic filters are incorporated into the the inner-loop control to eliminate the coefficient explosion problem of virtual signal differentiation. By treating the coupling term as a perturbation, the semi-global practical stability of the closed-loop system is established. Finally, the effectiveness of the obtained results are demonstrated by numerical simulations.

Keywords: unmanned aerial vehicle; maneuvering control; double dynamic filter

1. Introduction

As typical aerial mobile robots, quadrotor unmanned aerial vehicles (UAVs) are widely used in national defense, exploration, and industrial transportation, owing to their compact size, high flexibility, and strong durability. Among the various tasks involving UAVs, trajectory tracking for predefined targets has garnered significant research interest worldwide. In UAV control research, the classical methods are applicable to relatively simple flight tasks. By contrast, advanced control strategies, including neural-dynamics-based control [1, 2], fixed-time control [3, 4], event-triggered control [5, 6], prescribed performance control [7–9], sliding mode control [10–12], active disturbance rejection control [13, 14], exhibit prominent superiority in improving system stability and robustness. Furthermore, the integration of UAV trajectory tracking with cooperative control [15–18] has achieved remarkable performance in a variety of practical applications.

Unlike trajectory tracking, numerous practical applications require UAVs to follow a specified path. To accommodate dynamic behaviors such as speed and acceleration, UAVs must be capable of adapting

their motion state accordingly, which gives rise to the maneuvering problem [19, 20]. In essence, the maneuvering problem is typically decomposed into two distinct tasks. The primary task involves geometric constraints, requiring the UAV to reach and maintain the predefined path. The secondary task pertains to dynamic behavior, encompassing time allocation, velocity, or acceleration management along the path. The maneuvering control of UAVs, whose attitude subsystem is described by a rotation matrix, has been explored in [21, 22]. It is worth noting that the rotation matrix, as a singularity-free attitude representation form, suffers from computational redundancy in control design. By contrast, Euler angles not only reduce dimensionality but also provide a more intuitive physical interpretation. Consequently, this motivates the present work to formulate maneuvering control of UAVs based on Euler angles to characterize the attitude equation.

As is well known, UAVs are typical underactuated and strongly coupled systems. Based on the structural characteristics of quadrotors, hierarchical control methods have been proposed in several studies [23–26]. The UAV system was transformed into two cascaded linear subsystems in [23], and through a novel stability analysis, it was proved that the closed-loop system is locally exponentially stable under the coupling effect of nonlinear interconnections. The trajectory tracking problem of quadrotor aircraft subject to input saturation constraints was addressed in [25], where an inner–outer-loop hybrid control approach based on nested saturation was proposed. The advantage of hierarchical control lies in its clear system structure, and the incorporation of various constraints within the hierarchical subsystems can effectively achieve controller design. Nevertheless, the presence of the coupling term between the rotational and translational subsystem renders controller design and stability analysis highly intricate. In this paper, the adaptive maneuvering control problem of a UAV with geometric constraints and unknown parameters is designed. Based on the hierarchical framework, the underactuated quadrotor is transformed into a fully actuated system with explicit coupling terms. Rather than arbitrarily neglecting the coupling term in practical engineering [27], this work adopts rational analysis and appropriate treatment to obtain semi-global practical stability of the closed-loop system.

The main innovations of this paper are summarized as follows:

1) For UAV systems with unknown parameters and geometric constraints, based on vector backstepping, an adaptive static controller is designed in the outer-loop control to achieve the geometric task of the position subsystem. Meanwhile, a filter-gradient-update law is designed to accomplish the dynamic task.

2) Drawing on hierarchical control, the underactuated UAV system is transformed into a fully actuated system with a coupling term, which can be treated as a disturbance term. Unlike the complicated stability analysis in [23], appropriate parameters are selected, and Lyapunov analysis is adopted to establish the semi-global practical stability of the closed-loop system.

3) To overcome the explosion of terms in the inner-loop control, double dynamic filters are chosen. Compared with the command filter in [28], the double dynamic filters remove the the compensation signals and the assumption of bounded filtering errors.

Notations: The partial differentiation is denoted as $f^x(x,y) = \partial f/\partial x$, $f^{x^2}(x,y) = \partial^2 f/\partial x^2$. diag$\{\cdot\}$ represents a diagonal matrix. For a matrix x, x^{-1} is the inverse matrix, $|x| = \sqrt{\sum_{i,j} x_{ij}^2}$ denotes the Frobenius norm. For convenience, $\cos(\cdot)$, $\sin(\cdot)$, and $\tan(\cdot)$ are abbreviated as $C_{(\cdot)}$, $S_{(\cdot)}$, and $T_{(\cdot)}$, respectively.

2. Description of the problem

The UAV shown in Figure 1 is regarded as a rotating rigid body, where $O_g(x_g, y_g, z_g)$ is the global coordinate system, and $O_b(x_b, y_b, z_b)$ represents the body reference frame, respectively. The wing length is l, the mass of UAV is denoted by m, and g is the gravitational acceleration.

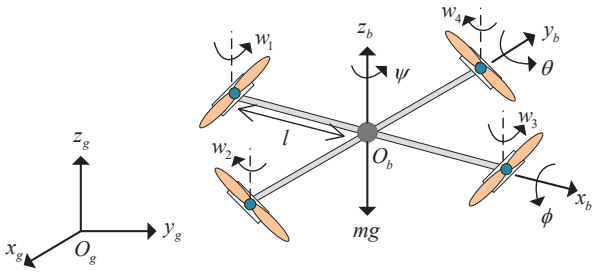

Figure 1. Reference frames of a UAV.

According to the principles of flight dynamics and aerodynamics [29, 30], the altitude and attitude motion of the UAV are described as follows:

$$\begin{aligned} \Sigma_k : &\begin{cases} \dot{r} = v, \\ m\dot{v} = uRe_3 - mge_3, \end{cases} \\ \Sigma_d : &\begin{cases} \dot{\eta} = H(\eta)\omega, \\ J\dot{\omega} = -S_k(\omega)J\omega + \tau, \end{cases} \end{aligned} \tag{2.1}$$

where $r = [x, y, z]^T$ and v denote the position and velocity of the UAV accordingly in $\{O_g\}$, the Euler angle vector (roll angle, pitch angle, yaw angle) along x_b, y_b, z_b-axis is $\eta = [\phi, \theta, \psi]^T$, and $e_3 = [0, 0, 1]^T$ is the unit vector. ω is the angular rate, and $\mathbf{J} = \text{diag}\{J_{xx}, J_{yy}, J_{zz}\}$ represents the moment inertia matrix. The operator $S_k(x) : \mathbb{R}^3 \to \mathbb{R}^{3\times3}$ is defined as $S_k(x)y = x \times y$ for $x, y \in \mathbb{R}^3$. $u \in \mathbb{R}$ and $\tau = [\tau_1, \tau_2, \tau_3]^T \in \mathbb{R}^3$ are the control force and torque applied on the UAV, respectively.

The rotation matrix $\mathbf{R}(\psi, \theta, \phi)$ and attitude kinematic matrix $\mathbf{H}(\eta)$ in system (2.1) are given by

$$\mathbf{R}(\eta) = \begin{pmatrix} C_\theta C_\psi & S_\phi S_\theta C_\psi - C_\phi S_\psi & C_\phi S_\theta C_\psi + S_\phi S_\psi \\ C_\theta S_\psi & S_\phi S_\theta S_\psi + C_\phi C_\psi & C_\phi S_\theta S_\psi - S_\phi C_\psi \\ -S_\theta & S_\phi C_\theta & C_\phi C_\theta \end{pmatrix}, \mathbf{H}(\eta) = \begin{pmatrix} 1 & S_\phi T_\theta & C_\phi T_\theta \\ 0 & C_\phi & -S_\phi \\ 0 & S_\phi/C_\theta & C_\phi/C_\theta \end{pmatrix}.$$

Considering the cascaded structure of the UAV, the system (2.1) can be regarded as an underactuated translational subsystem Σ_k and a fully actuated rotational subsystem Σ_d. Quadrotor UAVs feature superior flexibility and load-carrying capability, making them widely applicable in practical scenarios such as cargo transportation and agricultural spraying. Nevertheless, inherent uncertainties and time-varying characteristics of the payload mass necessitate the design of a dedicated controller to handle unknown mass parameters. The objective of this paper is to develop an adaptive inner–outer-loop controller to achieve the following objectives:

1) The desired path target set of the UAV can be characterized by such the constraint set

$$\mathcal{P} = \left\{ r \in \mathbb{R}^3 : \exists\, \varrho \in \mathbb{R} \text{ s.t. } r(t) = r_d(\varrho(t)) \right\},$$

where $r_d(\varrho) = [x_d(\varrho), y_d(\varrho), z_d(\varrho)]^T$ is a continuous parameterization of the path variable $\varrho(t)$. Different from trajectory tracking that imposes strict time constraints, the maneuvering control problem involves a geometric framework consisting of a geometric task and a dynamic task. Specifically, these two tasks refer respectively to the path $r(t)$ of system and velocity signal $\dot{\varrho}(t)$ of the path variable converging as closely as possible to the expected path $r_d(\varrho)$ and the expected speed assignment signal $v_s(\varrho, t)$, that is,

$$\begin{aligned} &\lim_{t\to\infty} |r(t) - r_d(\varrho(t))| \le \sigma_1, \\ &\lim_{t\to\infty} |\dot{\varrho}(t) - v_s(\varrho, t)| \le \sigma_2, \end{aligned} \tag{2.2}$$

where $\sigma_1, \sigma_2 > 0$.

2) The Euler angle $\eta = [\phi, \theta, \psi]^T$ tracks the desired angle $\eta_d = [\phi_d, \theta_d, \psi_d]^T$.

3) All signals in the error system are bounded.

For this end, the following three assumptions are given as follows:

Assumption 1. There exist constants $K_j > 0, (j = 1, 2)$ such that $|r_d^{\varrho^i}(\varrho)| \le K_1$ for $i \in \{0, 1, 2\}$, and $|v_s^{\varrho^i t^i}(\varrho, t)| \le K_2$ for $i \in \{0, 1\}$.

Assumption 2. The desired yaw angle ψ_d and its derivatives $\dot{\psi}_d, \ddot{\psi}_d$ are all bounded.

Assumption 3. The pitch angle satisfies $-\pi/2 < \theta < \pi/2$.

Remark 1. To ensure the smooth operation of the UAV, it is crucial to minimize drastic changes in the Euler angles during flight. The inclusion of Assumption 3, as mentioned in [31, 32], is imperative to ensure the reversibility of matrix $H(\eta)$. Moreover, the desired roll angle ϕ_d and desired pitch angle θ_d are provided by the attitude planner (see Eq (3.3)), whereas the user specifies the desired yaw angle ψ_d.

3. Controller design

In what follows, an adaptive maneuvering inner-outer-loop controller based on vector backstepping is presented to achieve the goals of this paper. The UAV is a typical strongly coupled system, and hierarchical control is commonly employed to address its position subsystem and attitude subsystem. The key of hierarchical control lies in the introduction of virtual control, which transforms the underactuated subsystem into a fully actuated subsystem with coupling term for processing.

The following subsections describe the design process of the inner–outer-loop controllers.

3.1. Outer-loop control

For the position dynamics equation Σ_k in (2.1), it can be naturally rendered to the following form:

$$\ddot{r} = \mu = kuR(\psi, \theta, \phi)e_3 - ge_3, \tag{3.1}$$

where $k = 1/m$ is an unknown parameter, and the estimation error is defined as $\tilde{k} = k - \hat{k}$. Introducing a formal virtual translational control vector $\mu_{\mathbf{d}}$ as

$$\mu_{\mathbf{d}} = u\hat{k}R_d(\psi, \theta_d, \phi_d)e_3 - ge_3, \tag{3.2}$$

which is used to extract the thrust u and the desired attitude angles θ_d, ϕ_d. Note that $\mu_{\mathbf{d}} = [\mu_{dx}, \mu_{dy}, \mu_{dz}]^T$ is to be given later, and ψ is the available yaw angle that can be fed back instantly. By inversely solving

(3.2), the desired thrust force and desired Euler angles can be computed as

$$\begin{aligned} u &= \frac{1}{\hat{k}}\sqrt{\mu_{dx}^2+\mu_{dy}^2+(\mu_{dz}+g)^2}, \\ \phi_d &= \arcsin(\frac{\frac{1}{\hat{k}}(\mu_{dx}S_\psi-\mu_{dy}C_\psi)}{u}), \\ \theta_d &= \arctan(\frac{\mu_{dx}C_\psi+\mu_{dy}S_\psi}{\mu_{dz}+g}). \end{aligned} \tag{3.3}$$

By comparing the expression of μ in (3.1) with $\mu_{\mathbf{d}}$ in (3.2), one obtains

$$\begin{aligned} \mu-\mu_{\mathbf{d}} &= u(kRe_3-\hat{k}R_de_3) \\ &= u(\tilde{k}Re_3+\hat{k}(Re_3-R_de_3)) \\ &= u\tilde{k}Re_3+\Delta, \end{aligned} \tag{3.4}$$

where Δ represents the interconnection term between the translation and rotation dynamics, which is given by

$$\Delta = 2u\hat{k}\begin{pmatrix} h_2C_\psi+h_3S_\psi & h_1C_\psi \\ h_2S_\psi-h_3C_\psi & h_1S_\psi \\ h_5 & h_4 \end{pmatrix}\begin{pmatrix} S_{\tilde{\phi}/2} \\ S_{\tilde{\theta}/2} \end{pmatrix},$$

the bounded continuous functions $h_i(\cdot),(i=1,\cdots,5)$ are the component of product of $S_{(\cdot)}$ and $C_{(\cdot)}$, which can be found in Appendix A.

Utilizing the vector backstepping, the design steps of the controller can be outlined as follows.

Step 1. For the position subsystem Σ_k, error transformations and speed assignment error are defined as

$$\begin{aligned} \tilde{r} &= r-r_d(\varrho), \\ \tilde{v} &= v-\alpha_1, \\ \omega_s(\dot{\varrho},\varrho,t) &= v_s(\varrho,t)-\dot{\varrho}, \end{aligned} \tag{3.5}$$

where $r_d(\varrho)=[x_d,y_d,z_d]^T$ is the desired position signal, and α_1 is the virtual control.

Choose the Lyapunov function as $V_1=\tilde{r}^T\tilde{r}/2$, based on (2.1) and (3.5), so that the virtual control law is designed as

$$\alpha_1 = -c_1\tilde{r}+r_d^{\varrho}v_s \tag{3.6}$$

with $c_1>0$. Then the derivative of V_1 turns to

$$\dot{V}_1 = -c_1\tilde{r}^T\tilde{r}+\tilde{r}^T\tilde{v}+\tilde{r}^Tr_d^{\varrho}w_s.$$

Step 2. Invoking (3.4), the derivative of velocity error $\tilde{v}$ in (3.5) is

$$\dot{\tilde{v}} = \mu_d+u\tilde{k}Re_3+\Delta+c_1\dot{\tilde{r}}-\alpha_1^{\varrho}\dot{\varrho}-\alpha_1^t, \tag{3.7}$$

where $\dot{\tilde{r}}=\tilde{v}-c_1\tilde{r}+r_d^{\varrho}\omega_s$, $\alpha_1^{\varrho}=r_d^{\varrho^2}v_s+r_d^{\varrho}v_s^{\varrho}$, $\alpha_1^t=r_d^{\varrho}v_s^t$.

Choose a Lyapunov function as

$$V_r = V_1+\frac{1}{2}\tilde{v}^T\tilde{v}+\frac{1}{2\lambda\gamma}w_s^2+\frac{1}{2p}\tilde{k}^2 \tag{3.8}$$

with $p, \lambda, \gamma > 0$. Based on (3.7), the derivative of V_r can be organized as

$$\begin{aligned}\dot{V}_r =& -c_1\tilde{r}^T\tilde{r} + \tilde{v}^T(\tilde{r} + \mu_d + u\tilde{k}Re_3 + \Delta + c_1\tilde{v} - c_1^2\tilde{r} - \alpha_1^{\varrho}v_s - \alpha_1^t) \\ &+ \frac{1}{\lambda\gamma}w_s\dot{w}_s + (\tilde{r}^T r_d^{\varrho} + c_1\tilde{v}^T r_d^{\varrho} + \tilde{v}^T\alpha_1^{\varrho})w_s - \frac{1}{p}\tilde{k}\dot{\hat{k}};\end{aligned} \tag{3.9}$$

then, the virtual controller and adaptive law are obtained as

$$\mu_{\mathbf{d}} = -(c_1 + c_2)\tilde{v} - (1 - c_1^2)\tilde{r} + \alpha_1^{\varrho}v_s + \alpha_1^t, \tag{3.10}$$

$$\dot{\hat{k}} = -p(\hat{k} - \tilde{v}^T uRe_3), \tag{3.11}$$

where $c_2 > 0$. Recalling the expression of Δ in Appendix A, the term $\tilde{v}^T\Delta$ in (3.9) becomes

$$\begin{aligned}\tilde{v}^T\Delta =& \ \tilde{v}_1\Delta_1 + \tilde{v}_2\Delta_2 + \tilde{v}_3\Delta_3 \\ \leq& \ 2\tilde{v}_1\hat{k}u((h_2C_\psi + h_3S_\psi)|S_{\tilde{\phi}/2}| + h_1C_\psi|S_{\tilde{\theta}/2}|) \\ &+ 2\tilde{v}_2\hat{k}u((h_2S_\psi - h_3C_\psi)|S_{\tilde{\phi}/2}| + h_1S_\psi|S_{\tilde{\theta}/2}|) + 2\tilde{v}_3\hat{k}u(h_4|S_{\tilde{\phi}/2}| + h_5|S_{\tilde{\theta}/2}|) \\ \leq& \ \tilde{v}_1\hat{k}u((h_2C_\psi + h_3S_\psi)\tilde{\phi} + h_1C_\psi\tilde{\theta}) + \tilde{v}_2\hat{k}u((h_2S_\psi - h_3C_\psi)\tilde{\phi} + h_1S_\psi\tilde{\theta}) + \tilde{v}_3\hat{k}u[h_4\tilde{\phi} + h_5\tilde{\theta}] \\ \leq& \ \frac{1}{4d}\hat{k}^2u^2|\tilde{v}|^2(h_1^2 + h_2^2 + h_3^2 + h_4^2 + h_5^2) + d(3|\tilde{\theta}|^2 + 5|\tilde{\phi}|^2) \\ \leq& \ \frac{3}{4d}\hat{k}^2u^2|\tilde{v}|^2 + 5d|\tilde{\eta}|^2,\end{aligned} \tag{3.12}$$

where $d > 0$, $\tilde{\eta} = \eta - \eta_d$ is the Euler angle error. The mathematical relationships $h_2^2 + h_3^2 + h_5^2 \leq 1$ and $h_1^2 + h_4^2 \leq 2$ are applied in (3.12). Incorporating (3.10)–(3.12) into (3.9) gives

$$\begin{aligned}\dot{V}_r \leq& -c_1|\tilde{r}|^2 - (c_2 - \frac{3\hat{k}^2}{4d}u^2)|\tilde{v}|^2 + 5d|\tilde{\eta}|^2 - \frac{1}{2}\tilde{k}^2 + \frac{1}{2}k^2 + \frac{1}{\lambda\gamma}w_s\dot{w}_s \\ &+ (\tilde{r}^T r_d^{\varrho} + c_1\tilde{v}^T r_d^{\varrho} + \tilde{v}^T\alpha_1^{\varrho})w_s.\end{aligned} \tag{3.13}$$

Remark 2. Borrowing from [23], the underactuated position subsystem is transformed into a fully actuated subsystem with a coupled term via the introduction of a virtual control vector. This technique can be extended to other underactuated systems, such as nonholonomic mobile robots and unmanned surface vehicles. For the desired rotation matrix $\mathbf{R_d}$, timely feedback of the yaw angle is employed instead of the desired yaw angle, to better characterize the actual flight situation.

Remark 3. To facilitate practical controller design in engineering applications, the coupling term Δ is commonly neglected, as reported in [27]. The existence of the coupling term Δ makes achieving pure feedback linearization for the translation subsystem challenging, and obtaining global stability is also difficult. The asymptotic stability of the whole error system is established in [23] by assuming that the coupling term satisfies the linear growth condition and adopting the cascade system theory.

3.2. Inner-loop control

In this part, the Euler angle tracking task of the attitude equation Σ_d is accomplished through the design of a torque controller.

Step 3. The error transformations can be defined as

$$\begin{aligned} \tilde{\eta} &= \eta - \alpha_{2d} = \eta - \alpha_2 - b_1, \\ \tilde{\omega} &= \omega - \alpha_{3d} = \omega - \alpha_3 - b_2, \end{aligned} \tag{3.14}$$

where $\alpha_2 = \eta_d = [\phi_d, \theta_d, \psi_d]^T$, and the filter errors are $b_1 = \alpha_{2d} - \alpha_2$, $b_2 = \alpha_{3d} - \alpha_3$. Notice that the differentiation of ϕ_d and θ_d in (3.3), which are composed of inverse trigonometric functions, is very complex. To avoid taking derivatives of α_2, α_3, inspired by [28], a novel double dynamic surface filter is employed, respectively, replacing α_2, α_3 with α_{2d}, α_{3d}, that is,

$$\begin{aligned} \dot{\zeta}_{i1} &= \kappa_i(-\zeta_{i1} + \zeta_{i2}), \\ \dot{\zeta}_{i2} &= \kappa_i(-\zeta_{i2} + \alpha_i), \\ \alpha_{id} &= \zeta_{i1},\ i = 2, 3, \end{aligned} \tag{3.15}$$

where $\kappa_i, (i = 2, 3)$ are time constants.

Defining the Lyapunov function $V_3 = \tilde{\eta}^T\tilde{\eta}/2$, along (2.1) and (3.14), we can arrive at

$$\dot{V}_3 = \tilde{\eta}^T(H(\eta)(\tilde{\omega} + \alpha_3 + b_2) - \dot{\alpha}_{2d}). \tag{3.16}$$

Choosing the virtual control as

$$\alpha_3 = H^{-1}(\eta)(-c_3\tilde{\eta} + \dot{\alpha}_{2d}), \tag{3.17}$$

where $c_3 > 0$, (3.16) turns into

$$\dot{V}_3 = -c_3\tilde{\eta}^T\tilde{\eta} + \tilde{\eta}^T(H(\eta)(\tilde{\omega} + b_2)).$$

Step 4. Choose a Lyapunov function as

$$V_\omega = V_3 + \frac{1}{2}\tilde{\omega}^T\tilde{\omega}, \tag{3.18}$$

whose derivative satisfies

$$\dot{V}_\omega = -c_3\tilde{\eta}^T\tilde{\eta} + \tilde{\eta}^T H(\eta)b_2 + \tilde{\omega}^T(J^{-1}(-S_k(\omega)J\omega + \tau) - \dot{\alpha}_{3d} + H^T(\eta)\tilde{\eta}). \tag{3.19}$$

The final torque control law is synthesized as

$$\tau = J(-c_4\tilde{\omega} + \dot{\alpha}_{3d} - H^T(\eta)\tilde{\eta}) + S_k(\omega)J\omega \tag{3.20}$$

with $c_4 > 0$, which implies that (3.19) can be written as

$$\dot{V}_\omega = -c_3|\tilde{\eta}|^2 - c_4|\tilde{\omega}|^2 + \tilde{\eta}^T H(\eta)b_2. \tag{3.21}$$

To clearly illustrate the design procedure of the inner–outer-loop controller, the structural block diagram is presented in Figure 2. The bounded tracking signals ϕ_d and θ_d generated by the outer loop are fed back to the inner loop, and the translational dynamics equation Σ_k depends on the rotation matrix $\mathbf{R}(\psi, \theta, \phi)$ defined by the inner loop. Meanwhile, in the design process of the inner-loop controller, the incorporation of a double dynamic surface filter circumvents complex derivative operations.

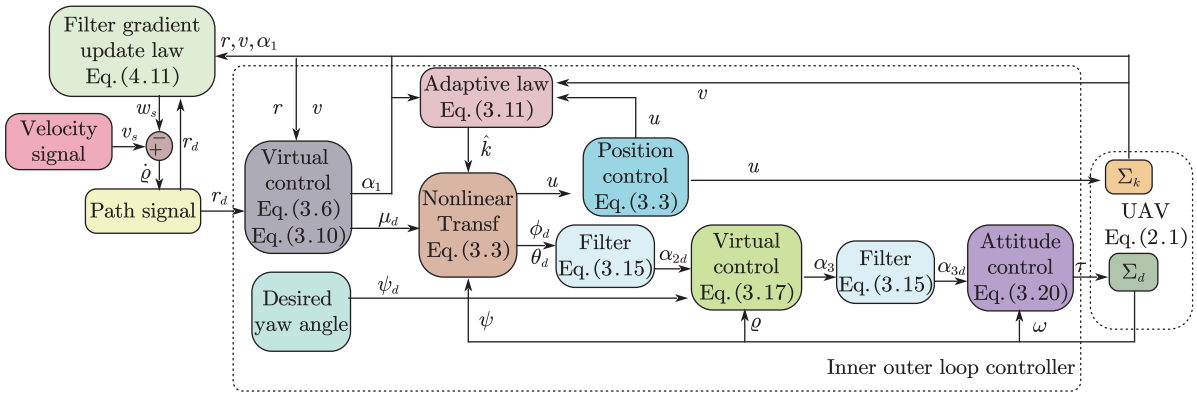

Figure 2. Block diagram of hierarchical control.

Remark 4. To avoid the derivation of virtual control signals, the double dynamic surface filter (3.15) is employed. Compared with the command filter in [28], the advantage of the double dynamic surface filter is to remove compensation signals and the general boundedness assumption of filter errors. In the subsequent stability analysis, the semi-global practical stability of the closed-loop system is obtained via appropriate error transformation and Lyapunov stability analysis, avoiding the use of singular perturbation theory to analyze the equilibrium point of the boundary layer system.

4. Stability analysis

In this section, an exhaustive stability analysis of the UAV system with the proposed inner-outer-loop controller is carried out. Define

$$\begin{aligned} z_{i1} &= \zeta_{i1} - \alpha_i, \\ z_{i2} &= \zeta_{i2} - \alpha_i, \end{aligned} \tag{4.1}$$

for $i = 2, 3$, where $z_i = [z_{i1}, z_{i2}]^T$. Based on (3.15), one has

$$\begin{aligned} \dot{z}_{i1} &= \kappa_i(z_{i2} - z_{i1}) - \dot{\alpha}_i, \\ \dot{z}_{i2} &= -\kappa_2 z_{i2} - \dot{\alpha}_i, \end{aligned} \tag{4.2}$$

which can be organized into a compact form:

$$\dot{z}_i = -\begin{pmatrix} \kappa_i & -\kappa_i \\ 0 & \kappa_i \end{pmatrix}\begin{pmatrix} z_{i1} \\ z_{i2} \end{pmatrix} - \begin{pmatrix} 1 \\ 1 \end{pmatrix}\dot{\alpha}_i := -B_1 z_i - B_2\dot{\alpha}_i, \ i = 2, 3. \tag{4.3}$$

For the filter error subsystem, choose the Lyapunov function $V_z = z_2^T z_2/2 + z_3^T z_3/2$, whose derivative can be presented as

$$\dot{V}_z \leq -\sum_{i=2}^{3}(\frac{1}{2}\kappa_i z_i^T z_i + (z_{i1} + z_{i2})\dot{\alpha}_i). \tag{4.4}$$

Considering (3.13), (3.21), and (4.4), the dynamic of the whole Lyapunov function $V = V_r + V_\omega + V_z$ is

$$\begin{aligned}\dot{V} \leq & -c_1|\tilde{r}|^2 - (c_2 - \frac{3\hat{k}^2}{4d}u^2)|\tilde{v}|^2 + \dot{w}_s(\frac{1}{\lambda\gamma}w_s + \tilde{r}^T r_d^o + c_1\tilde{v}^T r_d^o + \tilde{v}^T\alpha_1^o) - (c_3 - 5d)|\tilde{\eta}|^2 \\ & - c_4|\tilde{\omega}|^2 + \tilde{\eta}^T H(\eta)z_3 - \sum_{i=2}^{3}(\frac{1}{2}\kappa_i z_i^T z_i + (z_{i1} + z_{i2})\dot{\alpha}_i) - \frac{1}{2}\tilde{k}^2 + \frac{1}{2}k^2.\end{aligned} \tag{4.5}$$

Define the set of the states $\chi = (\tilde{r}^T, \tilde{v}^T, \tilde{\eta}^T, \tilde{\omega}^T, w_s, \tilde{k}, z_2^T, z_3^T)^T$. Noting the fact $|\mu_{\mathbf{d}}| = \sqrt{\mu_{dx}^2 + \mu_{dy}^2 + \mu_{dz}^2}$, and using (3.3), (3.10), and Assumption 1, we can find that

$$\begin{aligned}(u\hat{k})^2 = & \ \mu_{dx}^2 + \mu_{dy}^2 + (\mu_{dz} + g)^2 \\ & \leq 2|\mu_d|^2 + 2g^2 \\ & \leq 8[(c_1 + c_2)^2|\tilde{v}|^2 + (1 - c_1^2)^2|\tilde{r}|^2 + (\alpha_1^o v_s)^2 + (\alpha_1^t)^2] + 2g^2 \\ & \leq 8[(c_1 + c_2)^2|\tilde{v}|^2 + (1 - c_1^2)^2|\tilde{r}|^2 + (2K_1K_2^2)^2 + (K_1K_2)^2] + 2g^2 \\ & \leq d_a V + d_b,\end{aligned} \tag{4.6}$$

where $d_a = 16\max\{(c_1+c_2)^2, (1-c_1^2)^2\}$, $d_b = 32(K_1K_2^2)^2 + 8(K_1K_2)^2 + 2g^2$. Thus, the second term of the inequality (4.5) becomes $(c_2 - 3(d_aV + d_b)/4d)|\tilde{v}|^2$. Let it satisfy $c_2 - 3(d_aV + d_b)/4d - 2/d_1 \geq (1-\varepsilon)c_2 > 0$ with $0 < \varepsilon < 1, d_1 > 0$, to obtain

$$V(\chi) \leq v_0 = \frac{4d\varepsilon c_2 - 3d_b}{3d_a}, \tag{4.7}$$

where $c_2 > 3d_b/4d\varepsilon$. For the Lyapunov function V, one has

$$a_1|\chi|^2 \leq V(\chi) \leq a_2|\chi|^2, \tag{4.8}$$

where $a_1 = 0.5\min\{1, 1/p, 1/(\lambda\mu)\}$, $a_2 = 0.5\max\{1, 1/p, 1/(\lambda\mu)\}$. For constant $v_0 > 0$, define $r_0 = \sqrt{v_0/a_2}$, based on the definition of V, the initial value satisfies

$$|\chi(0)| \leq r_0 = \sqrt{\frac{4d\varepsilon c_2 - 3d_b}{3d_a a_2}}. \tag{4.9}$$

Consider the ball $B(0, r_0) = \{\chi : |\chi(0)| \leq r_0\}$ as a compact set, where the constants $e_{ij}, (i = 2, 3, j = 1, \cdots, 7)$ can always be found to satisfy the following inequality:

$$|\dot{\alpha}_i| \leq e_{i1}|\tilde{r}| + e_{i2}|\tilde{v}| + e_{i3}|\tilde{\eta}| + e_{i4}|\tilde{\omega}| + e_{i5}|z| + e_{i6}|w_s| + e_{i7}.$$

Thus, (4.5) can be transformed into

$$\begin{aligned}\dot{V} \leq & -(c_1 - \frac{2}{d_1})|\tilde{r}|^2 - (1 - \varepsilon)c_2|\tilde{v}|^2 - (c_3 - 5d - \frac{1}{2}|H(\eta)|^2 - \frac{2}{d_1})|\tilde{\eta}|^2 - (c_4 - \frac{2}{d_1})|\tilde{\omega}|^2 \\ & + w_s(\frac{1}{\lambda\gamma}\dot{w}_s + \tilde{r}^T r_d^o + c_1\tilde{v}^T r_d^o + \tilde{v}^T\alpha_1^o + \frac{2}{d_1}w_s) - (\frac{1}{2}\kappa_2 - q_2 - \frac{2}{d_1})|z_2|^2 \\ & - (\frac{1}{2}\kappa_3 - q_3 - \frac{2}{d_1} - \frac{1}{2})|z_3|^2 - \frac{1}{2}\tilde{k}^2 + \frac{1}{2}k^2 + \frac{2}{d_1},\end{aligned} \tag{4.10}$$

which employed

$$|(z_{i1}+z_{i2})\dot{\alpha}_i| \le q_i|z_i|^2 + \frac{1}{d_1}(|\tilde{r}|^2+|\tilde{v}|^2+|\tilde{\eta}|^2+|z|^2+|\tilde{\omega}|^2+|w_s|^2+1),\ i=2,3,$$

where $d_1>0$, $q_i = d_1\sum_{j=1}^{7} e_{ij}^2/4$. Accordingly, the filter-gradient-update law is set as

$$\dot{w}_s = -\lambda w_s - \lambda\gamma(\tilde{r}^T r_d^o + c_1\tilde{v}^T r_d^o + \tilde{v}^T\alpha_1^o + \frac{2}{d_1}w_s). \tag{4.11}$$

Further, the inequality (4.10) turns to

$$\begin{aligned}\dot{V} \le & -(c_1-\frac{2}{d_1})|\tilde{r}|^2 - (1-\varepsilon)c_2|\tilde{v}|^2 - \frac{1}{\gamma}w_s^2 - (c_4-\frac{2}{d_1})|\tilde{\omega}|^2 - (c_3-5d-\frac{1}{2}|H|^2-\frac{2}{d_1})|\tilde{\eta}|^2\\ & -(\frac{1}{2}\kappa_2-q_2-\frac{2}{d_1})|z_2|^2 - (\frac{1}{2}\kappa_3-q_3-\frac{2}{d_1}-\frac{1}{2})|z_3|^2 - \frac{1}{2}\tilde{k}^2+\frac{1}{2}k^2+\frac{2}{d_1}\\ \le & -cV+\delta.\end{aligned} \tag{4.12}$$

Let $c_1 = c_{11}+c_{12}$, $c_3 = c_{31}+c_{32}$, $c_4 = c_{41}+c_{42}$, $\kappa_2 = \kappa_{21}+\kappa_{22}$, $\kappa_3 = \kappa_{31}+\kappa_{32}$, where $c = \min\{2c_{11}, 2(1-\varepsilon)c_2, 2\lambda, 2c_{31}, 2c_{41}, \kappa_{21}, \kappa_{31}, 2p\}$, $\bar{c} = 2\min\{c_{12}-2/d_1, c_{32}-5d-|H|^2/2-2/d_1, c_{42}-2/d_1, \kappa_{22}/2-q_2-2/d_1, \kappa_{23}/2-q_3-2/d_1-1/2\}$, $\delta = k^2/2+2/d_1$. To make $c>0, \bar{c}>0$, it needs

$$\begin{aligned}&c_{11}>0, c_{12}>\frac{2}{d_1}, c_2>0, c_{31}>0, c_{32}>5d+\frac{1}{2}|H|^2+\frac{2}{d_1}, c_{41}>0,\\ &c_{42}>\frac{2}{d_1}, \kappa_{21}>0, \kappa_{22}>2q_2+\frac{4}{d_1}, \kappa_{31}>0, \kappa_{32}>2q_3+\frac{4}{d_1}+1.\end{aligned} \tag{4.13}$$

Up to now, the closed-loop dynamics system is expressed as

$$\begin{aligned}\dot{\tilde{r}} =& -c_1\tilde{r}+\tilde{v}+r_d^o\omega_s,\\ \dot{\tilde{v}} =& -c_2\tilde{v}-\tilde{r}+u\tilde{k}Re_3+\Delta+c_1r_d^o w_s+\alpha_1^o w_s,\\ \dot{\tilde{k}} =& p(\hat{k}-\tilde{v}^T uRe_3),\\ \dot{w}_s =& -\lambda w_s-\lambda\gamma(\tilde{r}^T r_d^o+c_1\tilde{v}^T r_d^o+\tilde{v}^T\alpha_1^o+\frac{2}{d_1}w_s),\\ \dot{\tilde{\eta}} =& -c_3\tilde{\eta}+H(\eta)(\tilde{\omega}+b_2),\\ \dot{\tilde{\omega}} =& -c_4\tilde{\omega}-H^T(\eta)\tilde{\eta},\\ \dot{z}_i =& -B_1z_i-B_2\dot{\alpha}_i,\ i=2,3.\end{aligned} \tag{4.14}$$

Based on the aforementioned analysis, the main results of this paper can be summarized as the following theorem.

Theorem 1. For the UAV system described by (2.1), under Assumptions 1–3, with the virtual control law in (3.6), (3.10), and (3.17), the control law designed in (3.3), (3.20), filter-gradient-update law in (4.11), and adaptive law given in (3.11), satisfying parameter requirements (4.13), the closed-loop system (4.14) has the following performances:

1) The system (4.14) is semi-globally uniformly practically asymptotically stable;

2) The maneuvering problem and the Euler angle tracking problem are solved;

3) All the signals in the error system (4.14) are bounded.

Proof: Invoking (4.8) and (4.12), one has

$$\begin{aligned} a_1|\chi|^2 \leq & V(\chi) \leq a_2|\chi|^2, \\ \dot{V}(\chi) \leq & -cV + \delta, \end{aligned} \tag{4.15}$$

where $c = \min\{2c_{11}, 2(1-\varepsilon)c_2, 2\lambda, 2c_{31}, 2c_{41}, \kappa_{21}, \kappa_{31}, 2p\}$, $\delta = k^2/2 + 2/d_1$. From [33], we can draw a conclusion that the error system (4.14) is semi-globally uniformly practically asymptotically stable. Further, based on the Grönwall inequality, one has

$$V(\chi(t)) \leq V(\chi(0))e^{-ct} + \frac{\delta}{c}. \tag{4.16}$$

By choosing d_1, c big enough, the right-hand side of (4.16) is small, and combining (4.8), the maneuvering problem (2.2) is naturally achieved:

$$\begin{aligned} \lim_{t\to\infty} |r - r_d(\varrho)| \leq & \quad \sqrt{\tfrac{2\delta}{c}}, \\ \lim_{t\to\infty} |v_s(\varrho, t) - \dot{\varrho}| \leq & \quad \sqrt{\tfrac{2\lambda\gamma\delta}{c}}. \end{aligned}$$

Obviously, the signal χ is bounded, and due to the signals, $\tilde{\eta}$ is bounded, which implies that the Euler angle can track the desired signal.

According to Assumption 1, (3.3), (3.5), (3.6), and (3.10), the signals r, α_1, v, μ_d, u are bounded. Recalling Assumption 2 and (3.3), the desired angles ϕ_d, θ_d, ψ_d are bounded, which, equivalent to the fact that the tracking error η_d is bounded, η is bounded. The filter error signals z_2, z_3 in χ are bounded. For matrix $\mathbf{H}(\eta)$ and its inverse matrix $\mathbf{H^{-1}}(\eta)$, the Frobenius norms meet $|\mathbf{H}(\eta)| = \sqrt{1 + 2\sec^2\theta}$, $|H^{-1}(\eta)| = \sqrt{3}$; further, from (3.14), (3.17), and (3.20), the signals α_3, ω, τ are also bounded.

Remark 5. In [28, 34], the existence and uniqueness of the isolated equilibrium of command filter is assumed for stability analysis based on singular perturbation theory. Specifically, the equations

$$\zeta_{i1} = \alpha_i, \ \ \zeta_{i2} = 0, \tag{4.17}$$

should have a unique isolated solution. In nonlinear systems, it is difficult to check this assumption, and thus, in this section, the equilibrium point problem of (4.17) is avoided by introducing the transformation (4.1).

5. Simulation

The effectiveness of the proposed controller is validated via quadrotor UAV simulations in this section. The desired path signal is given as $r_d(\varrho) = [x_d(\varrho), y_d(\varrho), z_d(\varrho)]^T = [\cos(0.1\varrho), 2\sin(0.1\varrho), 1 + 2\arctan(0.2\varrho)]^T$, where ϱ is an independent parametrization variable, and the desired speed signal of the path variable is set to

$$v_s(\varrho, t) = \frac{0.2\sin(0.05t)}{\sqrt{(x_{\mathrm{d}}^{\varrho}(\varrho))^2 + (y_{\mathrm{d}}^{\varrho}(\varrho))^2 + (z_{\mathrm{d}}^{\varrho}(\varrho))^2}}.$$

The parameters of UAV are $m = 2$, $g = 9.8$, $J_{xx} = J_{yy} = J_{zz} = 0.005$. The initial values are $r(0) = [0, 0, 0.5]^T$, $v(0) = [0, 0, 0]^T$, $\eta(0) = [0, 0, 0]^T$, $\omega(0) = [0, 0, 0]^T$, $\hat{k}(0) = 0.8, \varrho(0) = 0, w_s(0) = 0$. The

control design parameters are $c_1 = 0.25, c_2 = 0.8, c_3 = 0.6, c_4 = 0.4$, $d_1 = 5$, and the parameters of the gradient-update law are chosen as $\lambda = 0.5, \gamma = 0.4$. The adaptive gain is $p = 0.05$. In the filters, the initial values are selected as $\zeta_{21}(0) = \zeta_{22}(0) = \zeta_{31}(0) = \zeta_{41}(0) = [0, 0, 0]^T$, and the time constants are set as $\kappa_2 = \kappa_3 = 20$.

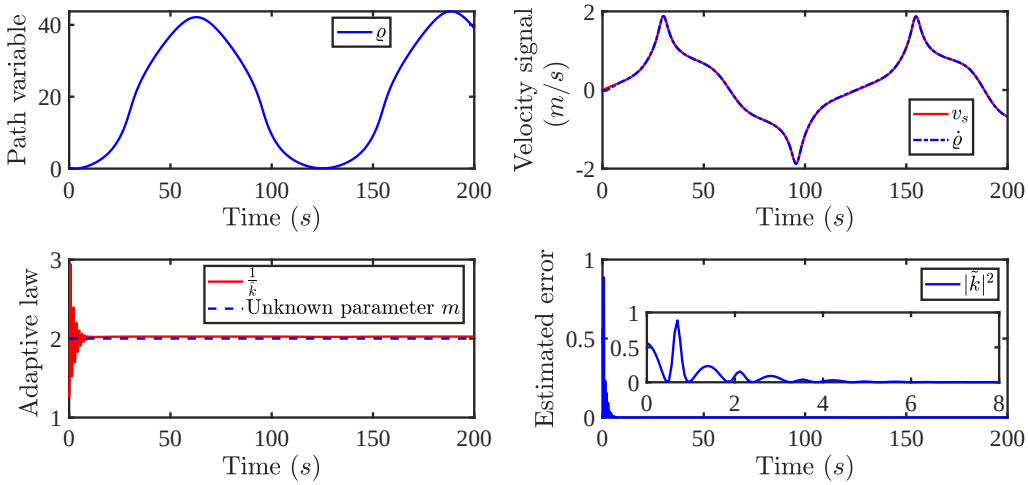

Figure 3. Speed signal and adaptive law.

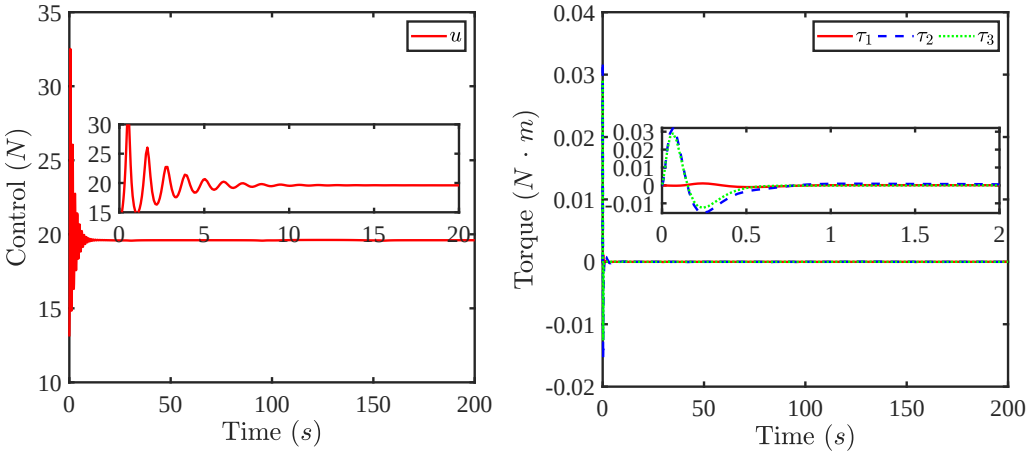

Figure 4. Control and torque.

As depicted in Figure 3, the velocity signal $\dot{\varrho}$ of the path variable converges to the desired velocity signal v_s, verifying that the dynamic task of the maneuvering task is satisfied. The corresponding estimation results for the unknown mass parameter $1/k = m = 2$ are presented in Figure 3. As illustrated in the last two subplots, the proposed adaptive law achieves accurate parameter identification. The squared estimation error $|\tilde{k}|^2$ exhibits a fast transient response: After an initial bounded peak, the error is rapidly suppressed and settles to a near-zero steady state with negligible residual oscillations, confirming both the transient performance and rapid convergence of the parameter estimation.

As shown in Figure 4, the response curves of the four control signals of the UAV are presented, including the lift force u and the torques τ_1, τ_2, τ_3. The lift force u exhibits a bounded transient re-

sponse, undergoing a brief oscillatory adjustment before converging smoothly to a steady-state value. The torques remain uniformly bounded with small magnitudes throughout the simulation, their initial transients decaying rapidly to near-zero steady-state values.

As shown in Figure 5, under the proposed bounded controller, the path output signal $r = [x, y, z]^T$ of the UAV converges to the desired reference path $r_d = [x_d, y_d, z_d]^T$. The position error $|\tilde{r}|^2$ exhibits a fast transient response and rapidly decays to near zero, verifying the successful completion of the geometric task. The attitude tracking performance is presented in Figure 6. The desired roll angle is specified as $\psi_d = 0.1\cos(0.1t)$; the Euler angles $\eta = [\phi, \theta, \psi]^T$ accurately track their desired references $\eta_d = [\phi_d, \theta_d, \psi_d]^T$. The attitude tracking error $|\tilde{\eta}|^2$ also decays rapidly to a negligible neighborhood of zero, confirming that the attitude tracking objective is achieved simultaneously.

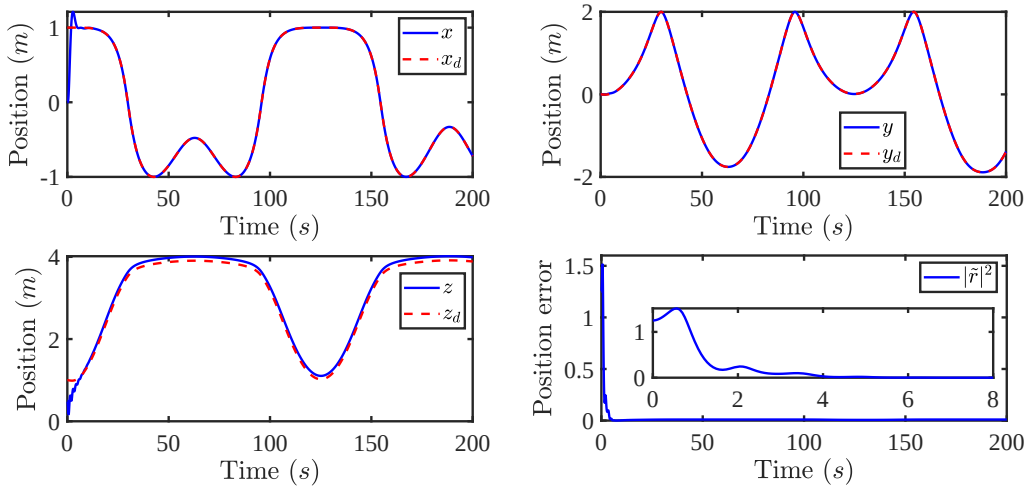

Figure 5. Position and position error.

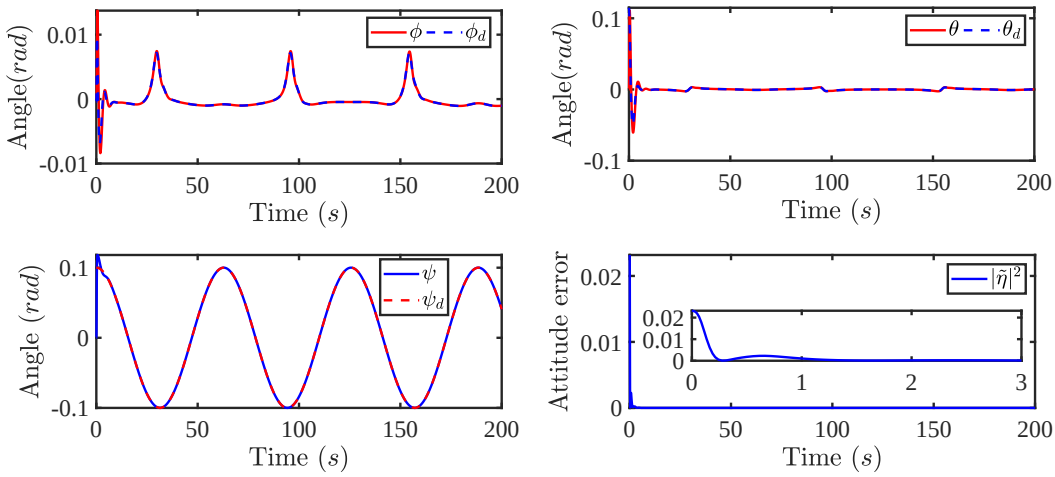

Figure 6. Euler angles and attitude error.

6. Conclusions

This paper focuses on the development of an adaptive maneuvering inner-outer-loop control for a quadrotor UAV with filter techniques. For the position subsystem and attitude subsystem, inner–loop and outer-loop controllers are designed separately to achieve maneuvering tasks and Euler angle tracking tasks, respectively. By appropriately scaling the coupling terms, the semi-global practical stability of the closed-loop system is obtained in stability analysis. Moreover, several relevant topics remain under ongoing investigation, including cooperative maneuvering control and safety control for multiple UAVs.

Use of AI tools declaration

The authors declare they have not used Artificial Intelligence (AI) tools in the creation of this article.

Acknowledgments

This work was supported by the Research Project Initiation Fund (BS202463), the Shandong Province Natural Science Foundation General Project (ZR2025MS19), and the Youth Innovation Team Program (2025KJH195).

Conflict of interest

The authors declare that they have no known competing financial interests or personal relationships that could have appeared to influence the work reported in this paper.

References

1. L. N. Zheng, Z. J. Zhang, Convergence and robustness analysis of novel adaptive multilayer neural dynamics-based controllers of multirotor UAVs, *IEEE Trans. Cybern.*, **51** (2021), 3710–3723. https://doi.org/10.1109/TCYB.2019.2923642
2. L. N. Zheng, F. Q. Deng, Z. L. Yu, Y. M. Luo, Z. J. Zhang, Multilayer neural dynamics-based adaptive control of multirotor UAVs for tracking time-varying tasks, *IEEE Trans. Syst. Man Cybern. Syst.*, **52** (2022), 5889–5900. https://doi.org/10.1109/TSMC.2021.3130748
3. J. Olguin-Roque, S. Salazar, I. González Hernandez, R. Lozano, A robust fixed-time sliding mode control for quadrotor UAV, *Algorithms*, **16** (2023), 229. https://doi.org/10.3390/a16050229
4. M. Khodaverdian, S. Hajshirmohamadi, A. Hakobyan, S. Ijaz, Predictor-based constrained fixed-time sliding mode control of multi-UAV formation flight, *Aerosp. Sci. Technol.*, **148** (2024), 109113. https://doi.org/10.1016/j.ast.2024.109113
5. H. Z. Guo, M. Chen, Y. H. Shen, M. Lungu, Distributed event-triggered collision avoidance formation control for QUAVs with disturbances based on virtual tubes, *IEEE Trans. Ind. Electron.*, **72** (2025), 1892–1903. https://doi.org/10.1109/TIE.2024.3417975

6. X. B. Lin, J. Liu, Y. Yu, C. Y. Sun, Event-triggered reinforcement learning control for the quadrotor UAV with actuator saturation, *Neurocomputing*, **415** (2020), 135–145. https://doi.org/10.1016/j.neucom.2020.07.042
7. F. Hu, T. D. Ma, X. J. Su, Adaptive fuzzy sliding-mode fixed-time control for quadrotor unmanned aerial vehicles with prescribed performance, *IEEE Trans. Fuzzy Syst.*, **32** (2024), 4109–4120. https://doi.org/10.1109/TFUZZ.2024.3393763
8. L. F. Hua, W. H. Wang, K. B. Shi, J. Yang, Q. S. Zhong, H. J. Liang, Safety-critical fixed-time trajectory tracking of quadrotor UAVs via event-triggered prescribed performance sliding mode control, *IEEE Trans. Consum. Electron.*, **72** (2026), 1821–1830. https://doi.org/10.1109/TCE.2025.3650623
9. K. Liu, L. Jiao, Y. Zhang, P. Y. Zhao, Adaptive predefined-time prescribed performance control with application to a quadrotor UAV, *IEEE Trans. Aerosp. Electron. Syst.*, **62** (2026), 4751–4770. https://doi.org/10.1109/TAES.2026.3654056
10. O. Mofid, S. Mobayen, Robust fractional-order sliding mode tracker for quad-rotor UAVs: event-triggered adaptive backstepping approach under disturbance and uncertainty, *Aerosp. Sci. Technol.*, **146** (2024), 108916. https://doi.org/10.1016/j.ast.2024.108916
11. J. Baek, M. Kang, A synthesized sliding-mode control for attitude trajectory tracking of quadrotor UAV systems, *IEEE/ASME Trans. Mechatron.*, **28** (2023), 2189–2199. https://doi.org/10.1109/TMECH.2022.3230755
12. M. D. Golea, M. Lungu, R. Wang, D. G. Voinea, High-order disturbance observer-based backstepping sliding mode control of the under-actuated uncertain quadrotor unmanned aerial vehicles, in *2025 29th International Conference on System Theory, Control and Computing (ICSTCC)*, (2025), 679–684. https://doi.org/10.1109/ICSTCC66753.2025.11240397
13. L. X. Xu, H. J. Ma, D. Guo, A. H. Xie, D. L. Song, Backstepping sliding-mode and cascade active disturbance rejection control for a quadrotor UAV, *IEEE/ASME Trans. Mechatron.*, **25** (2020), 2743–2753. https://doi.org/10.1109/TMECH.2020.2990582
14. Z. J. Wang, T. Zhao, Based on robust sliding mode and linear active disturbance rejection control for attitude of quadrotor load UAV, *Nonlinear Dyn.*, **108** (2022), 3485–3503. https://doi.org/10.1007/s11071-022-07349-y
15. H. Liu, Y. F. Lyu, W. B. Zhao, Robust visual servoing formation tracking control for quadrotor UAV team, *Aerosp. Sci. Technol.*, **106** (2020), 106061. https://doi.org/10.1016/j.ast.2020.106061
16. H. Z. Guo, M. Chen, B. M. Li, Distributed event-triggered collision avoidance coordinated control for QUAVs based on flexible virtual tubes, *Chin. J. Aeronaut.*, **38** (2025), 103300. https://doi.org/10.1016/j.cja.2024.11.010
17. M. Jabeen, Q. H. Meng, H. R. Hou, H. Y. Li, Odor source localization in outdoor building environments through distributed cooperative control of a fleetof UAVs, *Expert Syst. Appl.*, **247** (2024), 123332. https://doi.org/10.1016/j.eswa.2024.123332
18. K. Liu, W. Y. Yang, L. Jiao, Z. P. Yuan, C. Y. Wen, Fast fixed-time distributed neural formation control-based disturbance observer for multiple quadrotor UAVs under unknown disturbances, *IEEE Trans. Aerosp. Electron. Syst.*, **61** (2025), 13137–13155. https://doi.org/10.1109/TAES.2025.3578046

19. R. Skjetne, T. I. Fossen, P. V. Kokotović, Robust output maneuvering for a class of nonlinear systems, *Automatica*, **40** (2004), 373–383. https://doi.org/10.1016/j.automatica.2003.10.010
20. R. Skjetne, T. I. Fossen, P. V. Kokotović, Adaptive maneuvering, with experiments, for a model ship in a marine control laboratory, *Automatica*, **41** (2005), 289–298. https://doi.org/10.1016/j.automatica.2004.10.006
21. D. Cabecinhas, R. Cunha, C. Silvestre, A globally stabilizing path following controller for rotorcraft with wind disturbance rejection, *IEEE Trans. Control Syst. Technol.*, **23** (2015), 708–714. https://doi.org/10.1109/TCST.2014.2326820
22. S. Z. Wu, X. Liang, Y. C. Fang, W. He, Geometric maneuvering for underactuated VTOL vehicles, *IEEE Trans. Autom. Control.*, **69** (2024), 1507–1519. https://doi.org/10.1109/TAC.2023.3324268
23. F. Kendoul, Nonlinear hierarchical flight controller for unmanned rotorcraft: design, stability, and experiments, *J. Guid. Control Dyn.*, **32** (2009), 1954–1958. https://doi.org/10.2514/1.43768
24. R. Naldi, M. Furci, R. G. Sanfelice, L. Marconi, Robust global trajectory tracking for underactuated VTOL aerial vehicles using inner-outer loop control paradigms, *IEEE Trans. Autom. Control*, **62** (2016), 97–112. https://doi.org/10.1109/TAC.2016.2557967
25. L. Martins, C. Cardeira, P. Oliveira, Global trajectory tracking for quadrotors: An MRP-based hybrid strategy with input saturation, *Automatica*, **162** (2024), 111521. https://doi.org/10.1016/j.automatica.2024.111521
26. M. Micu, M. Lungu, M. Chen, M. R. Ebrahimpour, Four-stage cascaded control scheme based on robust nonlinear dynamic inversion technique for quadrotors, in *2024 28th International Conference on System Theory, Control and Computing (ICSTCC)*, (2024), 235–240. https://doi.org/10.1109/ICSTCC62912.2024.10744662
27. M. R. Mokhtari, B. Cherki, A. C. Braham, Disturbance observer based hierarchical control of coaxial-rotor UAV, *ISA Trans.*, **67** (2017), 466–475. https://doi.org/10.1016/j.isatra.2017.01.020
28. J. A. Farrell, M. Polycarpou, M. Sharma, W. J. Dong, Command filtered backstepping, *IEEE Trans. Autom. Control*, **54** (2009), 1391–1395. https://doi.org/10.1109/TAC.2009.2015562
29. P. Castillo, R. Lozano, A. E. Dzul, *Modelling and Control of Mini-Flying Machines*, *Springer-Verlag*, 2005. https://doi.org/10.1007/1-84628-179-2
30. G. Cai, B. M. Chen, T. H. Lee, *Unmanned Rotorcraft Systems*, *Springer Science & Business Media*, London, 2011. https://doi.org/10.1007/978-0-85729-635-1
31. K. Yan, M. Chen, Q. X. Wu, B. Jiang, Extended state observer-based sliding mode fault-tolerant control for unmanned autonomous helicopter with wind gusts, *IET Control Theory Appl.*, **13** (2019), 1500–1513. https://doi.org/10.1049/iet-cta.2018.5341
32. K. Yan, M. Chen, Q. X. Wu, R. G. Zhu, Robust adaptive compensation control for unmanned autonomous helicopter with input saturation and actuator faults, *Chin. J. Aeronaut.*, **32** (2019), 2299–2310. https://doi.org/10.1016/j.cja.2019.06.001
33. C. Yang, Z. J. Wu, Adaptive robust maneuvering control for nonlinear systems via dynamic surface technique, *Nonlinear Dyn.*, **111** (2023), 8369–8381. https://doi.org/10.1007/s11071-023-08289-x

34. R. Rashad, A. Aboudonia, A. El-Badawy, A novel disturbance observer-based backstepping controller with command filtered compensation for a MIMO system, *J. Franklin Inst.*, **353** (2016), 4039–4061. https://doi.org/10.1016/j.jfranklin.2016.07.017

Appendix A

The relationship between μ and $\mu_{\mathbf{d}}$ is established in this appendix. In view of the definition of $\mathbf{R}(\psi, \theta, \phi)$, the components of μ in (3.1) are

$$\begin{aligned} \mu_x &= ku(C_\phi S_\theta C_\psi + S_\phi S_\psi), \\ \mu_y &= ku(C_\phi S_\theta S_\psi - S_\phi C_\psi), \\ \mu_z &= kuC_\theta C_\phi - g. \end{aligned} \tag{A.1}$$

At the same time, the components of $\mu_{\mathbf{d}}$ along x, y, z-axis in (3.2) are given as follows

$$\begin{aligned} \mu_{dx} &= \hat{k}u(C_{\phi_d} S_{\theta_d} C_\psi + S_{\phi_d} S_\psi), \\ \mu_{dy} &= \hat{k}u(C_{\phi_d} S_{\theta_d} S_\psi - S_{\phi_d} C_\psi), \\ \mu_{dz} &= \hat{k}uC_{\theta_d} C_{\phi_d} - g. \end{aligned} \tag{A.2}$$

Substituting the roll angle error and pitch angle error $\tilde{\phi} = \phi - \phi_d$, $\tilde{\theta} = \theta - \theta_d$ into (A.1), yields

$$\begin{aligned} \mu_x &= ku(C_{(\phi_d+\tilde{\phi})} S_{(\theta_d+\tilde{\theta})} C_\psi + S_{(\phi_d+\tilde{\phi})} S_\psi), \\ \mu_y &= ku(C_{(\phi_d+\tilde{\phi})} S_{(\theta_d+\tilde{\theta})} S_\psi - S_{(\phi_d+\tilde{\phi})} C_\psi), \\ \mu_z &= kuC_{(\phi_d+\tilde{\phi})} C_{(\theta_d+\tilde{\theta})} - g. \end{aligned} \tag{A.3}$$

Exploiting some useful relations between trigonometric functions, namely

$$\begin{aligned} S_{(a+b)} &= S_a + 2S_{\frac{b}{2}} C_{(a+\frac{b}{2})}, \\ C_{(a+b)} &= C_a - 2S_{\frac{b}{2}} S_{(a+\frac{b}{2})}, \end{aligned}$$

then some terms from (A.3) are transformed into

$$\begin{aligned} C_{(\phi_d+\tilde{\phi})} S_{(\theta_d+\tilde{\theta})} &= (C_{\phi_d} - 2S_{\tilde{\phi}/2} S_{(\phi_d+\tilde{\phi}/2)})(S_{\theta_d} + 2S_{\tilde{\theta}/2} C_{(\theta_d+\tilde{\theta}/2)}) \\ &= C_{\phi_d} S_{\theta_d} + 2h_1 S_{\tilde{\theta}/2} + 2h_2 S_{\tilde{\phi}/2}, \\ S_{(\phi_d+\tilde{\phi})} &= S_{\phi_d} + 2h_3 S_{\tilde{\phi}/2}, \\ C_{(\phi_d+\tilde{\phi})} C_{(\theta_d+\tilde{\theta})} &= (C_{\phi_d} - 2S_{\tilde{\phi}/2} S_{(\phi_d+\tilde{\phi}/2)})(C_{\theta_d} - 2S_{\tilde{\theta}/2} S_{(\theta_d+\tilde{\theta}/2)}) \\ &= C_{\phi_d} C_{\theta_d} + 2h_4 S_{\tilde{\theta}/2} + 2h_5 S_{\tilde{\phi}/2}, \end{aligned} \tag{A.4}$$

where the expressions of $h_i(\cdot), (i = 1, \cdots, 5)$ are

$$\begin{aligned} h_1 &= C_{\phi_d} C_{(\theta_d+\tilde{\theta}/2)} - S_{\tilde{\phi}/2} S_{(\phi_d+\tilde{\phi}/2)} C_{(\theta_d+\tilde{\theta}/2)}, \\ h_2 &= -S_{\theta_d} S_{(\phi_d+\tilde{\phi}/2)} - S_{\tilde{\theta}/2} S_{(\phi_d+\tilde{\phi}/2)} C_{(\theta_d+\tilde{\theta}/2)}, \\ h_3 &= C_{(\phi_d+\tilde{\phi}/2)}, \\ h_4 &= -C_{\phi_d} S_{(\theta_d+\tilde{\theta}/2)} + S_{\tilde{\phi}/2} S_{(\phi_d+\tilde{\phi}/2)} S_{(\theta_d+\tilde{\theta}/2)}, \\ h_5 &= -C_{\theta_d} S_{(\phi_d+\tilde{\phi}/2)} + S_{\tilde{\theta}/2} S_{(\phi_d+\tilde{\phi}/2)} S_{(\theta_d+\tilde{\theta}/2)}. \end{aligned}$$

Substituting (A.4) into (A.3), and comparing with (A.2), leads to

$$\begin{aligned}
\mu_x &= \mu_{dx} + u\tilde{k}Re_3 + 2u\hat{k}\left[\left(h_2C_\psi + h_3S_\psi\right)S_{\tilde{\phi}/2} + h_1C_\psi S_{\tilde{\theta}/2}\right] \\
\mu_y &= \mu_{dy} + u\tilde{k}Re_3 + 2u\hat{k}\left[\left(h_2S_\psi - h_3C_\psi\right)S_{\tilde{\phi}/2} + h_1S_\psi S_{\tilde{\theta}/2}\right] \\
\mu_z &= \mu_{dz} + u\tilde{k}Re_3 + 2u\hat{k}\left[h_4S_{\tilde{\theta}/2} + h_5S_{\tilde{\phi}/2}\right],
\end{aligned}$$

which can be rewritten as

$$\mu = \mu_d + u\tilde{k}Re_3 + \Delta, \tag{A.5}$$

where

$$\Delta = 2u\hat{k}\begin{pmatrix} h_2C_\psi + h_3S_\psi & h_1C_\psi \\ h_2S_\psi - h_3C_\psi & h_1S_\psi \\ h_5 & h_4 \end{pmatrix}\begin{pmatrix} S_{\tilde{\phi}/2} \\ S_{\tilde{\theta}/2} \end{pmatrix}.$$